STRUCTURAL SIMILARITY BETWEEN WALL-BOUNDED TURBULENT FLOWS

Scott E. Hommema and **Ronald J. Adrian***
Laboratory for Turbulence and Complex Flow
Department of Theoretical and Applied Mechanics
University of Illinois at Urbana-Champaign
Urbana, Illinois 61801
shommema@uiuc.edu and r-adrian@uiuc.edu

ABSTRACT

A template matching technique is developed to examine the similarity between coherent structures in different wall-bounded turbulent flows. Experimental data obtained from turbulent pipe flow, turbulent channel flow, turbulent boundary layer flow, and the atmospheric boundary layer are used to explore structural similarity. Results indicate that a small ensemble of structures extracted from one flow can faithfully reconstruct a velocity–time signature from other flows, even at far different Reynolds numbers. Individual structures are interpreted in the framework of the hairpin vortex packet paradigm of wall turbulence. The frequency with which these structures occur suggests they are a robust and highly significant element of the dynamics of wall-bounded turbulent flows.

INTRODUCTION

A number of novel and powerful analysis techniques (e.g. quadrant analysis, VITA, Fourier decomposition) have been applied to study temporally resolved point-wise velocity measurements of wall-bounded turbulent flows, but few have been successful in deducing spatial structure from the temporal data. Wallace et al. (1977) introduced a temporal averaging scheme in which individual patterns (a slow deceleration followed by a rapid acceleration) observed in velocity–time records were assigned a local, representative convection velocity. In this way, large patterns could be broken into potential subpatterns. A hierarchy of patterns and subpatterns could be observed, but the nature of these patterns with regard to vortical structures in the flow could not be ascertained.

Flow visualization studies have indicated the presence of large scale coherent structures within wall-bounded shear flows. The work of Brown and Thomas (1977), Bandyopadhyay (1980), and others has identified spatial patterns (e.g. inclined structures) that can be associated with the hairpin vortex. Flow visualization has been extended to very large Reynolds numbers (Hommema and Adrian, 2001) where similarly organized patterns in the wall region were observed. Although suggestive, flow visualizations such as these do not necessarily provide an unambiguous description of the coherent vortical structures within the flow.

Recent advances in planar measurement techniques such as particle image velocimetry (PIV) have allowed the researcher to obtain instantaneous spatial information on a plane of interest. Recent studies taking advantage of this experimental technique (c.f. Adrian et al., 2000) have identified coherent vortical structures (hairpin vortices) which align to form larger structures (hairpin vortex packets) through low to moderate Reynolds number boundary layers.

The relationship between the temporal patterns observed in thermal anemometry studies, and the spatial patterns observed in flow visualization and planar measurements has not been established. Here, we present an effort to utilize the spatial information provided by PIV measurements to understand the temporal signatures within thermal anemometry measurements in the context of coherent vortical structures.

EXPERIMENT

The four experimental datasets utilized in this study are summarized in Table 1. PIV data in the streamwise–wall-normal plane of a zero-pressure gradient turbulent boundary layer are available from the large-format film measurements reported in Adrian et al. (2000).

*This research was funded by a grant from the National Science Foundation Atmospheric Sciences Division.

Dataset	Type	Span	$\mathrm{Re}_\tau = u_\tau\delta/\nu$
BL	PIV	$3\delta \times 1.2\delta$	2216
Channel	PIV	$1H \times 1H$	1734
Pipe	TA	1.6 s	1782
ABL	TA	15 min	1.3×10^6
Noise	S	1.6 s[a]	1782[a]

[a]equivalent values

Table 1: Summary of experimental datasets utilized. BL: boundary layer; ABL: atmospheric boundary layer; PIV: particle image velocimetry; TA: thermal anemometry; S: synthetic

Digital PIV measurements in fully developed channel flow are available in Christensen (2001). X-film measurements in fully developed turbulent pipe flow are described in Hommema (2001). The anemometry data from the neutral atmospheric boundary layer were obtained in conjunction with the aforementioned visualization experiments (Hommema and Adrian, 2001).

A template matching technique was developed to compare the spatial structures captured in the PIV experiments (BL and channel) with the temporal structures observed in the anemometry measurements (atmospheric boundary layer (ABL) and pipe).

A typical PIV realization from a turbulent laboratory boundary layer (Adrian et al., 2000) is shown in Figure 1. Consider a probe (e.g. a hot-wire anemometer) fixed in space at $y/\delta = 0.2$, $x/\delta = 1.0$. As the flow field advects over the probe, a characteristic velocity signature would be observed. Note that in the figure, while space advances from left-to-right, time advances from right-to-left for a fixed probe. The spatial sampling frequency of the PIV measurement, Δx, and the line average of the streamwise velocity at the given wall-normal location, $\overline{u}$ are used to convert between space and time, $t = -x/\overline{u}$. We will use velocity signatures of this type with spatial and temporal lengths of δ and l_T, respectively, as an ensemble of N templates, T_i. Note that we have employed Taylor's frozen field hypothesis, which in this context implies that the coherent structures in the flow advect past the probe unaltered, to convert the spatial sequence contained in the PIV realization to a temporal signature.

Consider a velocity–time record (pipe or ABL) obtained via thermal anemometry at the same wall-normal location as the template. We break the time record into M windows of length l_T. Each window will be denoted u_j where $j = 1, 2, \ldots, M$. A low-pass filter downsampled the data, originally acquired at 20 kHz, to the equivalent temporal frequency

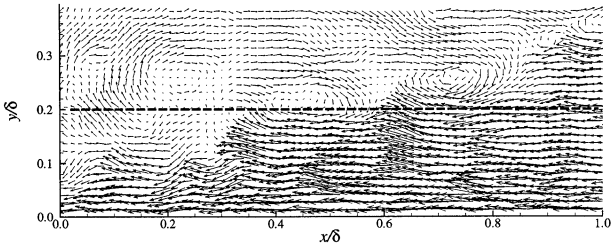

Figure 1: PIV realization from a turbulent laboratory boundary layer (Adrian et al., 2000). Mean flow is from left to right. A constant convection velocity ($0.8U_\infty$) has been subtracted from the vectors shown. A probe fixed at ($y/\delta = 0.2$) would record the velocity signature obtained by traveling along the dotted line from right to left.

Case	Template, T	M	Window, u	N
I	BL	149	Pipe	10,000
II	BL	149	ABL	100,000
III	Channel	100	Pipe	10,000
IV	Channel	100	ABL	100,000
V	Noise	149	Pipe	10,000
VI	Noise	149	ABL	100,000

Table 2: Six template matching cases considered.

of the template (typ. 500–600 Hz for the BL; 5–6 kHz for the channel). We define the correlation tensor between the ith PIV template and the jth anemometry window by

$$\rho_{ij} = \frac{\langle T_i u_j \rangle}{\sigma_{T_i}\sigma_{u_j}}, \qquad (1)$$

where the angle brackets denote an average and σ represents the root-mean-square (rms). When normalized in this manner, $|\rho_{ij}| \leq 1$, and a correlation coefficient of unity indicates perfect agreement between the spatial (PIV) and temporal (TA) signal. A small coefficient is indicative of little agreement.

A fifth dataset was synthetically generated to serve as a benchmark for the computed correlation coefficients. A signal was constructed with the same energy distribution (spectrum), mean, and rms fluctuation as the real turbulent signal, but without the coherence. To this end, a filter was generated from the measured streamwise velocity spectrum of fully developed turbulent pipe flow and applied to a white noise sequence. The resulting time series was low-pass filtered to coincide with the PIV dataset of interest and converted from a spatial to a temporal sequence. This time series was split into M windows, u_j, for use in the analysis given in the following section.

RESULTS

The template matching procedure was carried out for the six cases outlined in Table 2.

The correlation of a single template (e.g.

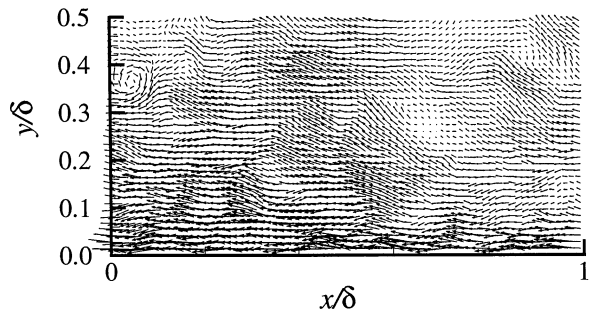

Figure 2: Representative BL template ($i = 47$) used in template matching analysis.

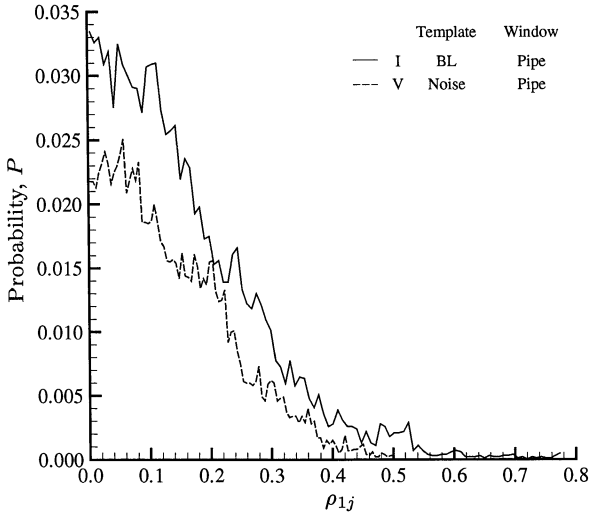

Figure 3: Representative probability histogram for Cases I and V at $y/\delta = 0.2$. In both cases, a single template (Figure 2) was correlated with 10,000 windows.

the first template) to a series of windows is denoted by ρ_{1j}. A probability distribution of the correlation values for Cases I and V for the single template shown in Figure 2, is given in Figure 3. Note that the highest correlation value obtained for Case V is 0.50, while for a real turbulent signal (Case I), the correlation reaches values as high as 0.78. Furthermore, $P_I(\rho) > P_V(\rho)$ for all values of the correlation coefficient. This is possible because although an equal number of windows were used for the analysis, the correlation for a real signal (Case I) is asymmetric (positive skewness) with respect to zero. This inequality suggests that the coherence of the turbulent signal plays an important role in the correlations. Similar results were obtained for the channel and ABL (Cases II-IV and III-VI) but are omitted here for brevity.

It proves interesting to examine those windows which yield the highest correlations with a given template. One such instance for Case I at $y/\delta = 0.2$ has been plotted in Figure 4 where two relevant length scales have been indicated.

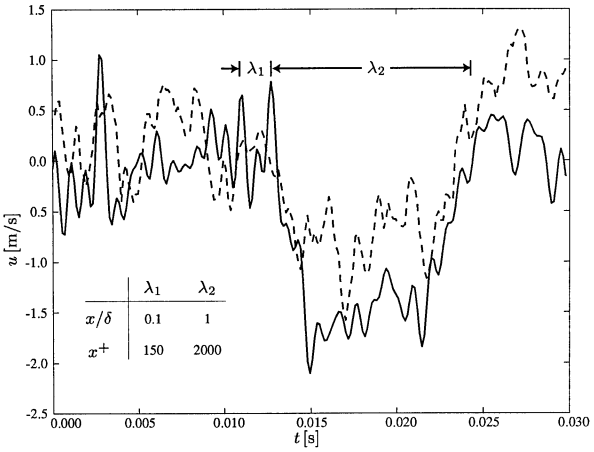

Figure 4: Window from Case I with highest correlation for $y/\delta = 0.2$. Approximate streamwise length of small and large-scale fluctuations indicated by λ_1 and λ_2, respectively. — Pipe window; - - BL template

We interpret these scales within the framework of the hairpin vortex packet paradigm. We associate the deviations of a small scale,λ_1, with the influence of a single hairpin vortex as it passes over the probe location. We associate the deviations of a larger scale, λ_2, with the passage of a hairpin vortex packet. Note that approximately six small-scale fluctuations (hairpin vortices) make up the large scale velocity fluctuation (hairpin vortex packet). For illustrative purposes, in Figure 4, a larger template with $l_T = 3\delta$ (approximately 30 ms) has been used.

In the case of channel flow (Case III) we are restricted to a template of $l_T = \delta$. The higher centerline velocity and smaller field-of-view restricts results in a record length of 2 ms. For the case shown in Figure 5 we find similar small scale velocity fluctuations with streamwise length 0.15δ. The field-of-view is insufficient to visualize fluctuations of scale λ_2.

The extremely large Reynolds number in the atmospheric boundary layer presents a number of problems related to the template matching analysis. First, the large Reynolds number is due mainly to the large length scale ($200 < \delta < 1000$ m). As a result, the ground-based instrumentation used in this work imposed a restriction of $y/\delta < 0.015$. More specifically, thermal anemometry data is available in the ABL for $y/\delta = 0.01$ and 0.07. The location of the data point closest to the wall (in inner and outer length scales), $y_{\min}$, for each of the three experimental apparatus is summarized in Table 3. We find that none of the laboratory experiments have sufficient resolution at the wall for scale similarity in δ. Likewise, if inner scaling is used, we find that none of the laboratory experiments have sufficient Reynolds number

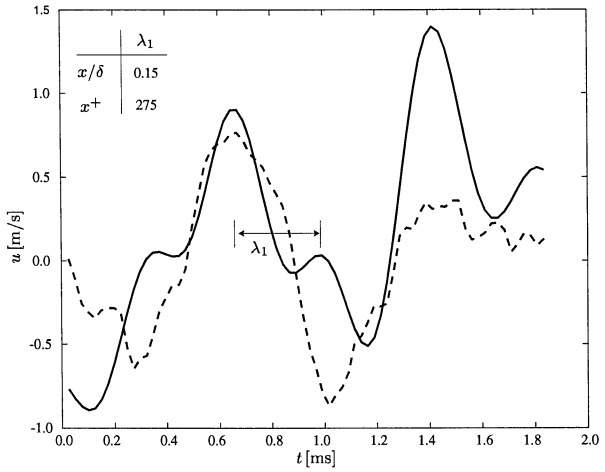

Figure 5: Window from Case III with highest correlation for $y/\delta = 0.2$. Approximate streamwise length of small-scale velocity fluctuations indicated by λ_1. — Pipe window; – – Channel template

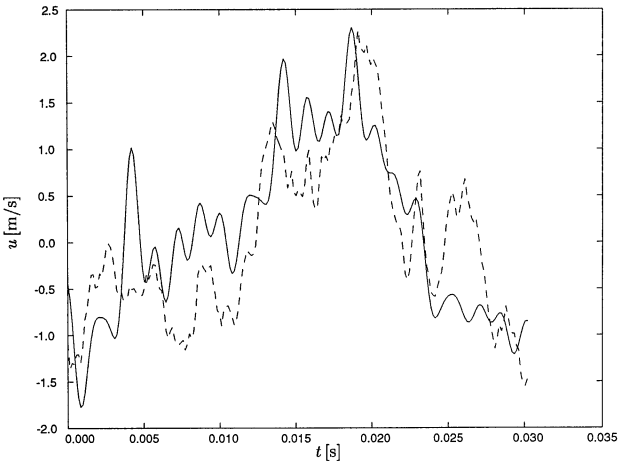

Figure 6: Window from Case II with highest correlation for $y/\delta = 0.01$. As discussed in the text, the template has been scaled along the time axis. — ABL window; – – Pipe template

to compare directly with the ABL. Therefore results analogous to those in Figures 3–5 cannot be computed *directly* for the ABL.

Instead, we use "template scaling" to account for the dissimilarity in Reynolds number and outer scale. In all cases discussed previously, we scale the templates along the temporal axis to account for differing convection velocities when Taylor's hypothesis was employed. In the case of the ABL, we perform additional scaling to account for the variation in outer scale between the window and the template. The template of interest is stretched or compressed along the time axis until the correlation is maximized. As expected, stretching (beyond that required from Taylor's hypothesis) was generally required. The measurements obtained in the ABL were at a much larger physical distance from the wall (c.f. Table 3) than for those obtained in the laboratory. As a result, we would expect structures with larger physical scales, and corresponding longer time scales in the ABL. One such result from the template scaling is shown in Figure 6 for Case II at $y/\delta = 0.01$. The value fo the correlation is 0.76, and we note a similarity in both the short and long time-scale fluctuations between the template and the window. It is remarkable that a template derived from a laboratory flow at far lower Reynolds number can correlate so well with data acquired in the ABL.

We use the results from an ensemble of templates to decompose the time records from thermal anemometry. Once the correlation tensor ρ_{ij} is formed we determine which templates correlate with the largest fraction of the windows. That is, for a given value of j we determine which template (i) provides the most

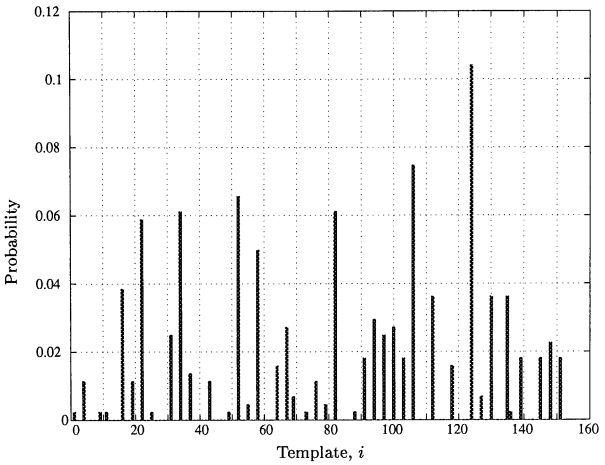

Figure 7: Probability distribution of templates with maximum correlation for BL template and pipe window at $y/\delta = 0.27$.

correlations that exceed 0.65. The probability distribution for a BL template and a pipe window (Case I) at $y/\delta = 0.27$ have been included in Figure 7. Only those templates whose correlations exceeded 0.65 (recall that for Case V the largest correlation obtained was 0.50) were considered in the decomposition.

We note two features in the histogram. First, the majority of the templates (111 out of 149) never correlate well (zero probability) with the pipe windows. Second, only eight to ten of the templates contribute significantly to the total probability. This is more easily distinguished by ordering the templates according to their probability and considering subsets of varying size. The results from such a decomposition are shown in Figure 8. The first eight templates are capable of reconstructing over 50% of the thermal anemometry signal. Moreover, the first 16 templates can reconstruct

	$y/\delta = 0.01$		$y/\delta = 0.007$		$y_{\min}$	
	y	y^+	y	y^+	y/δ	y^+
ABL	2.17 m	14,467	1.42 m	9,467	0.007	9,467
Channel	254 μm	17.4	178 μm	12.2	0.018	30.5
BL	831 μm	22.2	582 μm	15.5	0.014	30.2

Table 3: Summary of inner and outer length scales for experimental data sets.

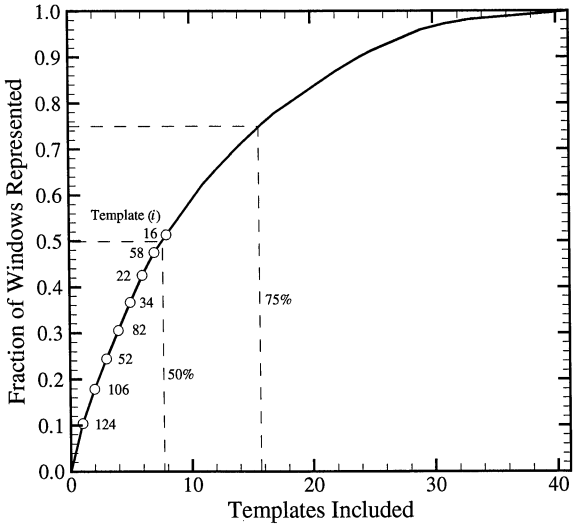

Figure 8: Cumulative fraction of windows from a single thermal anemometry record represented by a given number of templates. (Case I; $y/\delta = 0.27$)

75% of the signal.

The results shown in Figures 7 and 8 were computed from a single turbulent pipe flow realization. More striking results are obtained when an ensemble of 100 thermal anemometry realizations are used. Comparison between Figures 7 (singe realization) and 9 (100 realizations) reveal only minor differences in the distribution of the various templates. The cumulative represented fraction (see Figure 8 for the single realization case and Figure 10 for the 100 realization case) also reveals only minor changes. We find, as before, that only eight templates are required to represent 50% of the anemometry signals although the relative ordering of the required templates differs slightly. Only the first 17 templates (compare to 16 for the single realization case) are required to represent 75% of the windows. Decomposition of the entire ensemble requires an additional ten templates (51 total) when compared to the single realization.

It is of interest to examine the templates responsible for the majority of the decomposition. We deduce from Figures 9 and 10 that template number 124 is used most often in the decomposition of the velocity signal. This template has been reproduced in Figure 11. The

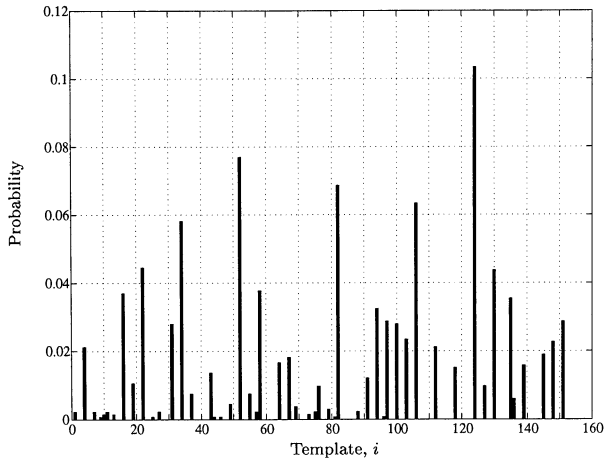

Figure 9: Probability distribution of templates with maximum correlation for a 100 realization ensemble from Case I at $y/\delta = 0.27$.

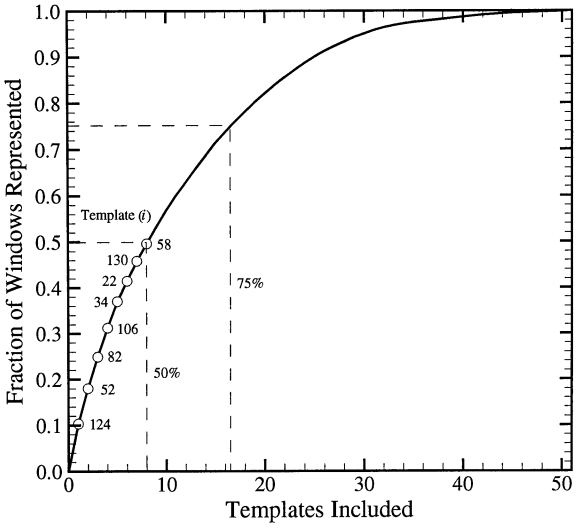

Figure 10: Cumulative fraction of windows from 100 thermal anemometry records represented by a given number of templates. (Case I; $y/\delta = 0.27$)

extent of a ramp-like feature has been indicated with a broken line. We interpret this feature as a hairpin vortex packet in the spirit of the paradigm in Adrian et al. (2000).

It is important to note that when viewed in the appropriate convective frame, the eight most probable templates identified in Figure 10 resemble hairpin vortex ramps of various sizes (interpreted as varying stages of development). These eight templates, although obtained from

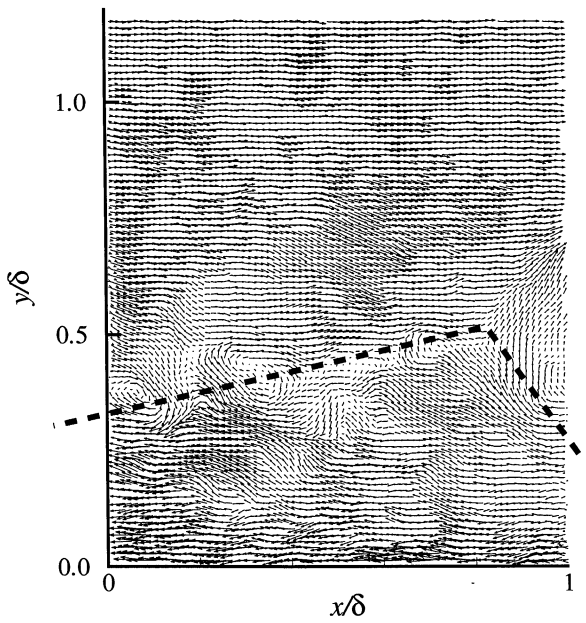

Figure 11: Most probable template (124) from the decomposition of Case I at $y/\delta = 0.27$. The extent of a ramp-like feature is indicated with a broken line.

a laboratory scale boundary layer, can reconstruct 50% of a velocity–time signal obtained in fully developed turbulent pipe flow, or even the first 3 m of the neutral atmospheric boundary layer. The additional nine templates required to reconstruct 75% of a velocity–time signal also resemble hairpin vortex ramps although the likeness becomes considerably more difficult to discern. This structural similarity between the various flows, and in the case of the ABL, at varying Reynolds number, suggests that the hairpin vortex ramps observed within the templates are a robust and significant feature of wall-bounded turbulent flows.

CONCLUSIONS

A template matching technique was developed to examine the structures common to wall-bounded turbulent flows. This technique compares spatial data obtained from particle image velocimetry experiments to the temporal data obtained from thermal anemometry. The template matching procedure was applied to data obtained in a turbulent boundary layer, fully developed turbulent channel flow, fully developed turbulent pipe flow, and the first 3 m of the neutral atmospheric boundary layer. Despite the different facilities, and in the case of the atmospheric boundary layer, despite the vast difference in Reynolds number, the observed structures were strikingly similar. It is conjectured that the time scales associated with the small and large scale velocity signatures observed in the templates are associated with the imprints of hairpin vortices and hairpin vortex ramps, respectively.

It is shown that an ensemble of time traces from fully developed turbulent pipe flow can be decomposed and reconstructed faithfully by a small number of candidate structures (templates). The structures contained within the templates can then be viewed as building blocks of the velocity–time signal obtained from thermal anemometry. Inspection of the most frequently utilized templates reveal ramp-like structures with downstream inclination which are interpreted as the signature of a hairpin vortex ramp.

REFERENCES

R. J. Adrian, C. D. Meinhart, and C. D. Tomkins. Vortex organization in the outer region of the turbulent boundary layer. *J. Fluid Mech.*, 422:1–54, 2000.

P. Bandyopadhyay. Large structure with a characteristic upstream interface in turbulent boundary layers. *Phys. Fluids*, 23(11):2326–2327, 1980.

G. L. Brown and A. S. W. Thomas. Large structure in a turbulent boundary layer. *Phys. Fluids*, 20:S243, 1977.

K. T. Christensen. *Experimental Investigation of Acceleration and Velocity Fields in Turbulent Channel Flow.* PhD thesis, Univeristy of Illinois at Urbana-Champaign, Urbana, Illinois, 2001.

S. E. Hommema. *Very-large Scale Motions in Wall-Bounded Turbulent Flows.* PhD thesis, Univeristy of Illinois at Urbana-Champaign, Urbana, Illinois, 2001. (in preparation).

S. E. Hommema and R. J. Adrian. Packet structure of surface eddies in the atmospheric boundary layer. *Boundary Layer Meterology*, 2001. (submitted).

J. M. Wallace, R. S. Brodkey, and H. Eckelmann. Pattern-recognized structures in bounded turbulent shear flows. *J. Fluid Mech.*, 83:673–693, 1977.